Pressure Consolidation of Amorphous ZrO_2-Al_2O_3 by Plastic Deformation of Powder Particles

A.S. Gandhi and V. Jayaram

Department of Metallurgy, Indian Institute of Science,

Bangalore 560 012, India

Abstract

Amorphous ZrO_2-Al_2O_3 powders undergo densification at low temperatures (<650°C) and moderate uniaxial pressures (~750 MPa). It is established that large pressure dependent densification and little time dependent densification occur. Viscous sintering is *not* the dominant densification mechanism. Study of the particle size effect in densification of amorphous ZrO_2-40% Al_2O_3, and comparison with hot pressing of borosilicate glass powder at 500 and 550°C and cold compaction of silver powder, clearly indicate the possibility of compaction of amorphous ZrO_2-Al_2O_3 by plastic deformation. Good agreement was seen between a model for the compaction of ductile metal powders and the observed hot pressing behaviour.

Keywords: *amorphous materials, powder consolidation, hot pressing, mechanical properties: plastic.*

1 INTRODUCTION

It has been previously reported that metastable amorphous ZrO_2-Al_2O_3 may be processed in bulk forms by low temperature pressure consolidation of amorphous powders produced by spray pyrolysis [1, 2, 3]. Bulk nanocrystalline metastable and stable microstructures have also been produced by crystallisation of the bulk amorphous material. Bulk processing of metastable ceramics, such as amorphous phases, and nanostructured and non-equilibrium crystalline phases is necessary for their characterisation and applications. However, densification of powders of the metastable ceramics through sintering with or without pressure is likely to lead to the transformation of the desired metastable phase into a more stable phase. In view of this problem, the ability to densify the amorphous ZrO_2-Al_2O_3 powders, at temperatures lower than 650°C and uniaxial pressures up to 750 MPa, is of much significance. The true density of the amorphous phase is very low compared to the equilibrium crystalline state, e.g. amorphous ZrO_2-40% Al_2O_3 has a density of 3.4 gcm^{-3} whereas the equilibrium microstructure consisting of monoclinic ZrO_2 and α-Al_2O_3 has a density of 5 gcm^{-3}. **It was hypothesised that the low true density and the more open structure that it implied might result in a material that was less viscous or otherwise more easily deformable and thereby make it possible for the amorphous powder to undergo large densification without crystallisation.** In the present investigation, the densification characteristics of amorphous ZrO_2-Al_2O_3 have been studied with the aim of identifying the dominant densification mechanism.

Densification, or sintering, in amorphous inorganic materials is generally expected to be governed by viscous deformation of the particles driven by capillary forces. The material may or may not be Newtonian viscous. The key feature of viscous sintering is that densification is time dependent. Viscous sintering for a Newtonian viscous material was the first sintering

mechanism to be analytically modelled, by Frenkel [4] and by Mackenzie and Shuttleworth [5].

The Frenkel model deals with the initial stage of sintering, namely the growth of a neck between two spherical particles. The ratio of the neck radius x and the particle diameter R as a function of time t is

$$\frac{x}{R} = \left(\frac{3\gamma}{2\eta R}\right)^{1/2} t^{1/2} \tag{1}$$

where γ is the surface energy of the material and η is its viscosity. The change in the height L of the compact with initial height L_0 is then given as

$$\frac{\Delta L}{L_0} = -\left(\frac{3\gamma}{8\eta R}\right) t \tag{2}$$

with $\Delta L = L - L_0$, which is a linear dependence on time.

The Mackenzie-Shuttleworth model was derived for the final stage of sintering, which may be described as the shrinkage of a spherical cavity in a viscous matrix. The latter model is found to be applicable even in the intermediate stage of sintering [6]. The rate of densification $d\rho/dt$ is given as

$$\frac{d\rho}{dt} = \left(\frac{3\gamma}{2\eta R_0}\right)(1-\rho) \tag{3}$$

where ρ is the relative density and R_0 is the initial particle size.

Relatively few models have been developed that relate the relative density of a viscous material to the densification parameters in the presence of an externally applied pressure. One such model is the extension of the Mackenzie-Shuttleworth model, developed by Murray *et al*. [7]. Their equation can be written as [8]

$$\ln\left(1-\rho(t)\right) = \ln\left(1-p_c\right) + \frac{3P_a}{4\eta}t \tag{4}$$

with p_c being the capillary pressure (usually $2\gamma/R$) and P_a is the applied pressure.

A model for the intermediate stage of viscous sintering was developed by Scherer [9] who described the porous compact as an array of thin cylinders that increased in diameter and reduced in length under the action of capillary force. This model and the Mackenzie-Shuttleworth model agree with each other over a reasonably large range of intermediate relative density and are the generally accepted models of viscous sintering [6].

According to Jagota and Dawson [10], the model by Matthews [11] is satisfactorily applicable to the initial stage of densification. This model was developed for the sintering of a compact by a creep mechanism with a stress exponent 'n' and incorporates applied hydrostatic pressure. The densification rate is given as

$$\frac{\dot{\rho}}{\rho_0} = \frac{27\pi B}{4}\left(\frac{\rho-\rho_0}{3\rho_0}\right)^{\left(\frac{1}{2}-n\right)}\Psi^{\left(n+\frac{1}{2}\right)}\left(\frac{(2n-1)}{6n}\frac{\alpha_c\sigma}{\pi}\right)^n \tag{5}$$

where ρ_0 is the starting relative density, α_c is a geometric factor and σ is the applied hydrostatic pressure. Ψ is given as

$$\Psi = \left(\frac{2n}{2n+1}\right)^{2(n-1)}$$

B is the linear creep coefficient relating the uniaxial stress σ_u to the strain rate.

$$\dot{\varepsilon}_u = B\sigma_u^n$$

The exponent n = 1 and B = $1/\eta$ for a viscous material. Hence the relative density as a function of time for uniaxial hot pressing in a rigid die is given as

$$\left(\frac{\rho-\rho_0}{\rho_0}\right)^{3/2}=\frac{7.5P}{\eta}t \tag{6}$$

for a Poisson's ratio of 0.3 for the compact.

Scaling laws relating the characteristic length scale, namely the particle size, to the rate of sintering enable the distinction to be made between the various sintering mechanisms. The scaling law for viscous sintering has an exponent of 1 [6, 12]. If Δt_i is the sintering time for particle size R_i, then the scaling law for viscous sintering is given as

$$\frac{\Delta t_2}{\Delta t_1}=\frac{R_2}{R_1} \tag{7}$$

In contrast, sintering of a crystalline powder compact by grain boundary diffusion has the scaling law

$$\frac{\Delta t_2}{\Delta t_1}=\left(\frac{R_2}{R_1}\right)^4 \tag{8}$$

The sintering rate in a viscous sintering process is expected to have a reciprocal relation with the particle size.

In the present paper, results of hot pressing experiments on the amorphous ZrO_2-40% Al_2O_3 powders at temperatures between 300 and 600°C and pressures between 250 and 750 MPa are presented. Effect of particle size ranges, cold pressure, time of hot pressing, and crystallisation were studied to identify the densification mechanism of the amorphous powders. Comparisons were made with the densification of crystallised ZrO_2-Al_2O_3, borosilicate glass and silver powders. It will be shown in light of the viscous sintering models described above, that viscous deformation is *not* the dominant densification mechanism **at low temperatures** in amorphous ZrO_2-Al_2O_3.

2 Experimental Procedures

2.1 Powder Preparation

An aqueous solution of zirconium nitrate (Nuclear Fuel Complex, Hyderabad, India) and aluminium nitrate (Loba Chemie, Mumbai, India) corresponding to the composition ZrO_2-40% Al_2O_3 (Z40A) was sprayed onto a Teflon coated pan at 250°C. The resultant powder was fully decomposed into an amorphous oxide powder by calcination at 750°C for 1 hour. Particle size separation was carried out on the thermally decomposed powders by sedimentation in a 15 cm tall column of de-ionised water, to obtain up to three particle size ranges,

1. fine (F) particles with size smaller than 3 μm,
2. medium (M) particle size range between 3 and 15 μm, and
3. coarse (C) particle size range between 15 and 35 μm.

Borosilicate glass powder (Pyrex) of particle size smaller than 15μm was obtained by grinding glassware followed by sedimentation. Silver powder (Loba Chemie, Mumbai) was used for pressing experiments after light grinding with a mortar and a pestle to break the agglomerates. Scanning electron microscopy, SEM (JEOL JSM-840A) was done on the powders after coating with gold as needed, to measure the particle sizes.

2.2 Hot Pressing

Densification experiments were performed on powders of ZrO_2-40% Al_2O_3 using a die of superalloy 718 with 5 mm internal diameter, on a screw driven Instron testing machine. Most of the experiments began by cold pressing a powder sample weighing ~0.1 g by loading up to 50 MPa and holding the pressure for 5 minutes. The cold compaction pressure was chosen so

that a crack-free compact with a known low relative density could be produced. Cold compaction pressures up to 750 MPa were used in the set of experiments carried out to study the effect of cold compaction on the hot pressing behaviour. A graphite paste was used as a lubricant on the die wall. Discs of graphite with 0.2 mm thickness were placed between the powder and both the punches to prevent the powder entering the small clearance between the die wall and the punches. The following procedure was followed during cold pressing in order to know the exact weight of the cold compact:

The graphite paste was applied on the die wall and the bottom punch with the graphite disc placed. This assembly was weighed (w_1) after the paste had dried. About 0.1g powder was poured into the die and the weight recorded again (w_2). The top graphite disc was then placed and the weight recorded (w_3). Cold compaction was carried out at this stage. The top punch was removed and any loose powder sticking to the die was removed. The die assembly was weighed again (w_4). The weight of the powder compact, w_c, is given by

$$w_c = w_4 - w_3 + w_2 - w_1$$

The top punch was inserted and the die assembly containing the green compact was then heated to 300, 450 or 600°C at 20 to 30 °C/min. The die cavity temperature was calibrated separately. A pressure of 250, 500 or 750 MPa was applied after reaching the desired temperature, at a cross-head speed of 10 μm/s. **This pressure was manually kept constant upon reaching the desired value and was released after the desired time.** The pressure was released after the desired time, usually 1 hour. A temperature compensated extensometer was adapted for recording the sample thickness. Applied pressure, displacement and time were recorded at intervals of 0.4s.

Densification experiments were also conducted on borosilicate glass and silver powders. The weight of the powder compact was chosen such that the volume occupied by a 100% dense compact would be the same as in the experiments on ZrO_2-Al_2O_3. Cold pressing of the glass powder was performed at 50 MPa, followed by hot pressing. At 500°C, pressures of 50, 225 and 450 MPa were applied successively, at 15 minutes' intervals. Pressures of 10, 50, 225 and 450 MPa were used at 550°C.

Densification experiments were performed on silver powder at room temperature and at 406°C ($0.55T_m$). Initial compaction was performed with a pressure of 5 MPa. At room temperature, the compact was pressurised continuously up to 225 MPa and the pressure was held constant for 30 min. At 406°C, pressures of 5, 10 and 50 MPa were applied successively, at 15 minutes' intervals.

3 RESULTS AND DISCUSSION

3.1 Consolidation of amorphous ZrO_2-Al_2O_3

SEM micrographs of the powders used in this study are presented in Fig.1 and Fig.2. Such micrographs were used for measuring the particle sizes. All the powder particles, except the silver powder, were angular in shape. However, the larger particles in the C range had open void space. These particles are expected to be weaker, or friable, due to the open porosity than the finer particles which are dense.

The displacement and the load data obtained from a hot pressing or room temperature compaction experiment, were smoothened by using 3 points on either side of a datum point. The unloading portion represents elastic recovery in the entire set-up. The compliance of the

load train was significant because of the design of the temperature compensated extensometer. A polynomial of degree 5 was fitted to this portion by regression analysis. The resulting function was used for subtracting the elastic deformation from the displacement data. The sample thickness was converted into density from the weight and the diameter of the sample in the die. The recorded density was verified by measuring the density by Archimedes' principle and the porosity by image analysis of the polished samples. The values agree with each other within ±4% relative density. The reproducibility of the hot pressed density, measured was within ±3% relative density. The scatter in the hot pressed density is probably due to variation in the lubrication. The cold pressed density at 50 MPa was much more reproducible in all the particle sizes: Z40A F - 42.8 ± 0.7 %, M - 37 ± 1.0 % and C - 34.5 ± 0.2 %. Any small change in the true density of the amorphous phase during hot pressing is not significant in the context of studying the phenomenon of consolidation of the amorphous powders.

Fig.3 shows the relative density of the Z40A compacts with the fine particle size, at three temperatures. There are two parts of each hot pressing experiment: The first is the loading portion up to the point of attaining the desired pressure, while the second is holding the pressure constant. It has been already reported [3] that although the general characteristics of the densification curves for all the temperatures appear similar, all the samples pressed at 300°C were found not to have developed particle to particle bonding which the higher temperature experiments produced. The density increased by a few tens of percent of the true density as the pressure was applied, whereas very little time-dependent densification was observed in all the experiments on amorphous powders. This observation is an indication of a densification mechanism that is strongly pressure dependent and has a weak time dependent component. It is therefore implied that viscous sintering is not the dominant densification

mechanism and the occurrence of non-viscous, plastic deformation is suggested. We now examine this possibility in more details, first by a generic comparison of the data in (Fig.3) for amorphous ZrO_2-Al_2O_3 with consolidation in a glass and in a soft metal. The roles of particle size and prior cold compaction pressure are then examined. Finally, experimentally obtained flow stresses from uniaxial data are used in conjunction with a model for cold compaction of metal powders to predict the consilidation response of amorphous ZrO_2-Al_2O_3 and compare it with the hot pressing data.

3.2 Consolidation of Glass and Silver

Corroboration of the hypothesis that a process of plastic deformation is responsible for the densification of amorphous ZrO_2-Al_2O_3 was sought through generic comparisons of the density-pressure and density-time curves obtained from hot pressing experiments on borosilicate glass and silver powders, as well as cold compaction of the silver powder. Fig.4 shows the results of hot pressing of the borosilicate glass powder at 500°C. The glass transition temperature is 525°C. The experiment involved three increasing pressures, applied successively for periods of 15 minutes each. It was observed that the increment in density over 15 minutes as the pressure was held constant was comparable to, if not greater than, the increment during pressurising. For instance, at 500°C as the pressure was increased from 50 to 225 MPa, the relative density increased from 65 to 71%, and similar increment was seen over 15 minutes as the pressure was held constant at 225 MPa. At 550°C (figure not shown), corresponding increments were 67 to 73% and 73 to 84%. Similar behaviour was seen above and below the glass transition temperature of **525°C**, although the densification at 550°C was higher than at 500°C. The contrast is clear between the densification behaviour of borosilicate glass, which is well known to sinter by viscous flow, and that of amorphous ZrO_2-Al_2O_3 (Fig.3).

Fig.5 presents the plots of the relative density of silver compact at room temperature as a function of increasing pressure. The relative density rose from 35 to 86%. The time dependent component of densification was small but measurable (2%, from 86 to 88%) and may be due to creep of silver since the applied pressure was quite high. The similarity is obvious between the curves for silver and that of amorphous ZrO_2-Al_2O_3.It is well known that silver powder, similar to other ductile metal powders, densifies through plastic deformation under externally applied pressure at room temperature. **Additional data, not reported here, on the compaction of silver powder at 0.55 homologous temperature (406°C) shows a general behaviour that is similar to that of the borosilicate glass, i.e. consolidation by creep is comparable to or greater than that due to monotonic increase in pressure. The above comparisons make it highly plausible that the primary behaviour seen in amorphous ZrO_2-Al_2O_3 is more of an athermal nature than one of creep, whether Newtonian or otherwise.**

3.3 Effect of Particle Size on Consolidation of Amorphous ZrO_2-Al_2O_3

The effect of particle size on the densification kinetics of the Z40A composition will now be analysed **with a view to understanding the mechanism in more detail. Viscous sintering mechanisms are known to depend on particle size, while no such dependence has been found for the cold compaction of soft metal powders that consolidate by slip deformation**. The time dependent component of densification being extremely small and of similar magnitudes in all the experiments, no scaling law involving time is applicable. The discussion is accordingly limited to the pressure dependence of relative density. The relative densities of the cold pressed compacts for the three particle sizes used in the present experiments decreased with increasing particle size (F - ~43%, M - 37% and C - 34.5%). The

fine powder compacts reached higher densities at 450 and 600°C than the two larger particle sizes during pressurising (Fig.6a and b), although the difference is small in view of the precision of the hot pressing experiments. The coarse powder compacts reached slightly higher densities than the medium particle size compact in spite of a lower starting density. This may be due to the highly porous large particles in the coarse powder that are likely to be friable. It was also seen that densification was possible in the fine powder compacts even below 50 MPa, which was the cold compaction pressure, while it was very small in the larger particle sizes. Furthermore, in spite of the monotonic decrease in initial density with increasing particle size, the increments in relative density ($\Delta\rho = \rho - \rho_0$, where ρ_0 is the initial % relative density) were of similar magnitudes in all the three compacts. **The implication of the above results is that the role of particle size is minor. We now examine the small differences in some detail.**

Fig.6 implies that at the higher temperatures of hot pressing, any given relative density was achieved at a lower pressure in the fine powder compact than the coarse powder compacts. This leads to an apparent particle size effect on the 'flow stress' of a porous compact for the same relative density; namely, compacts with larger pores are more difficult to densify. No established correlation of the pore size with the flow stress has been reported in the powder metallurgy literature. In the absence of a pore size effect, the coarse powder compacts would be expected to have a higher rate of densification with increasing pressure and finally coincide with the curve for the fine powder. Such merger of densification curves was observed during pressing at 300°C (Fig.6c). However, it must be remembered that no interparticle bonding, or sintering, took place in these experiments. Both types of behaviour have been reported for compaction of ductile metal powders. For instance, Park *et al.* reported the merger of density-pressure curves during the cold compaction of copper powders [13],

whereas Paramanand and Ramakrishnan [14] observed no such trend. **This apparent anomaly can be understood by** visualising the densification as an interplay of particle rearrangement, deformation and fragmentation. In the compaction of highly ductile powders, rearrangement and fragmentation are minimal, if present at all [15]. During compaction of very hard and brittle materials, such as oxide and carbide ceramics, fragmentation and rearrangement are likely to occur. However, in compaction of powders of hard metals, all the three processes are likely to occur at different stages. The contribution of the various processes is expected to be determined by the coefficient of friction between particles, the yield stress and the fracture strength of the particles. A transition is seen in the compaction of most metal powders, wherein the initial increase in the density is due to the rearrangement and deformation of particles while further increase is possible only by plastic deformation of the particles [15, 16, 17,]. The present experiments indicate similar behaviour, namely significant particle deformation, and possibly fragmentation, occurring once particle rearrangement becomes impossible. The particle size governs the different extents of re-arrangement and plastic deformation occurring in the compacts. Overall, it can be said that the particle size plays a weaker, albeit complicated role in compaction than in other sintering processes such as viscous sintering and sintering of crystalline ceramics. This feature lends support to the view that plastic deformation may be the **dominant** mechanism of densification.

3.4 Effect of Cold Compaction Pressure

The effect of cold compaction pressure on the hot pressing behaviour of amorphous Z40A is also of interest for establishing the role of plastic deformation in densification. The fine particle size always led to higher initial relative density. According to the analysis in the preceding paragraphs, a higher cold-compaction pressure is expected to reduce the extent of

re-arrangement possible during hot pressing, and little densification is expected till the applied pressure is adequate for deformation. A set of hot pressing experiments at 600°C on the fine powder with various cold compaction pressures was undertaken, the results of which are presented in Fig.7. No significant densification occurred till the pressure reached a certain value. The pressure for beginning the densification increased with increasing cold pressure, and was lower than the corresponding cold pressure. Once the densification began, the curves started to coincide, except for 500 and 750 MPa cold pressures. This anomaly is suspected to arise from cracks introduced during such high pressure cold compaction, although the density differences are small. It is clear from these experiments that for a given particle size range, the density-pressure curve is unique owing to the unique combination of particle re-arrangement, fragmentation and deformation.

3.4 Comparison with Cold Compaction Models

The results described so far conclusively establish that time dependent, viscous deformation is not the dominant mechanism of densification. It is therefore claimed that amorphous ZrO_2-Al_2O_3 deforms plastically at elevated temperatures. The results are in marked contrast to the densification of conventional glassy inorganic materials. The nature of the plastic deformation of the material is therefore of great interest and was studied in detail [18, 19]. The occurrence of plastic deformation in amorphous ZrO_2-Al_2O_3 was established by conducting uniaxial compression tests at 600 to 700°C in the strain rate range of $5x10^{-5}$ to 10^{-3} s^{-1}. The material exhibited elastic-plastic transition accompanied by sharp yield drop. Further plastic deformation occurred at a constant flow stress which was insensitive to strain rate. Up to 14% compressive plastic strain was without macroscopic failure was recorded. Consequently, a model that relates the yield behaviour of a ductile material to its compaction characteristics is expected to be applicable to the hot pressing experiments in the present work. The process of

compaction of a ductile powder has been modeled both empirically and analytically [20]. The earliest models [16, 17, 21, 22] are of the type

$$\ln\left(\frac{1}{1-\rho}\right) = KP + C \tag{9}$$

where ρ is the fractional relative density and P is the applied pressure. The constants K and C are related to the powder characteristics such as particle shape and size, and the material parameters such as the yield stress and hardening behaviour. These constants are determined empirically or analytically [23]. A model based on the observation that rearrangement occurs only initially and that the average particle co-ordination and the contact area increase during compaction was developed by Fischmeister and Arzt [24]. Yield surfaces for powder compacts in different states of stress such as uniaxial die pressing and isostatic pressing are modeled based on the von Mises yield criterion [25, 26, 27]. A simple model [25] which has been shown to fit hydrostatic compaction data well is

$$P_y = 3\rho^2\left(\frac{\rho-\rho_0}{1-\rho_0}\right)\sigma_y \tag{10}$$

where P_y is the macroscopic hydrostatic yield stress, ρ_0 is the initial relative density and σ_y is the uniaxial yield stress. The Cam-Clay model appears to be applicable to compaction under various states of stress [28] but it contains a few user-defined parameters. The particle size is not considered in the analytical models. Equation 10 has good agreement with the experimental data and will be used for analysing the present uniaxial compaction data, by estimating the hydrostatic component P_y for a given density and converting it into uniaxial pressure based on the following relation:

$$P_y = \frac{P}{3}\frac{(1+\upsilon)}{(1-\upsilon)} \tag{11}$$

where P is the uniaxial pressure and ν is the Poisson's ratio (assumed to be 0.3). Fig.8 shows the experimental uniaxial pressure as a function of relative density and the pressure calculated

from Equation 10 for the hot pressing of the fine and coarse powders at 600°C up to 750 MPa. Two values were used for the yield stress, 360 MPa corresponding to the average of the yield stress from all the compression tests and 240 MPa corresponding to the average flow stress after yield drop. The forms of the calculated curves appear similar to the experimental curves for both the particle sizes. The agreement between the model and experimental curves is as good as that encountered in the compaction of metal powders. The explanation of the densification behaviour of the amorphous ZrO_2-Al_2O_3 on the basis of plastic deformation of the particles is therefore vindicated.

It must be noted that the particle size is not considered in the models of compaction. The uniaxial pressure against the quantity $\rho^2(\rho-\rho_0)/(1-\rho_0)$ has been plotted for all the particle sizes at each temperature of hot pressing in Fig.9. The slope of the curve is $9(1+\nu)/(1-\nu)\sigma_y$. It is clear that at 450 and 600°C the plots are not straight lines, and are different for the three particle sizes. Interestingly, at 300°C the plots for the three particle sizes are straight lines that coincide. However, since no interparticle bonding occurs at 300°C, it is likely that the densification occurs without plastic deformation. The experiments at 300°C are therefore akin to cold compaction of a hard ceramic powders. Such compaction has been modeled in terms of yield criteria [29] with the 'yield stress' being determined by the interparticle friction or particle fracture strength. The straight lines in Fig.9c are expected if between rearrangement and fragmentation, one process dominates the other. Conversely, at the higher temperatures, the additional interaction of particle deformation with the other processes may lead to non-linear curves in Fig.9a and b. The particle size governs the exact nature of the interaction of the processes of rearrangement, fragmentation and deformation, leading to distinct curves for the three sizes at the higher temperatures.

It was pointed out that during hot pressing at a constant pressure time-dependent densification was very small and occurred mainly in the first few minutes. In order to identify any other influence of time on the hot pressed pellet, hardness was measured on polished samples which were hot pressed at 600 °C with a pressure of 750 MPa for various times up to 60 minutes. It is seen in Fig.10 that the hardness values for the samples hot pressed for successively longer times are higher. The hardness apparently reduced between 30 and 60 minutes. This is most probably an artefact of the damage during ejection caused by the stronger frictional locking of the compact with the die wall. Such locking was seen consistently in long hot pressing times, so that a sample pressed for 120 minutes could not be ejected without major damage. The increase in the hardness with hot pressing time may be due to improved bonding at the prior particle boundaries and recovery or relaxation process in the sample following deformation during pressurising.

4 CONCLUSIONS

The present investigation has established the role of non-viscous, plastic deformation in the densification of amorphous ZrO_2-Al_2O_3. The comparison of densification characteristics of this material with those of borosilicate glass around its T_g, and with silver at room temperature clearly point out the similarity with silver. Analysis of the particle size effect on densification from the standpoint of relative contribution of particle rearrangement, fragmentation and plastic deformation further supports the conclusion that plastic deformation is the dominant densification process. A fairly good agreement of a model for the cold compaction of ductile powders was obtained **with the observed trends in pressure-consolidation of amorphous ZrO_2-Al_2O_3 using a measured flow stress of 340 MPa and 260 MPa on the densified samples.**

Acknowledgements

Financial support for the present research was provided by the Department of Science and Technology, India. A.S. Gandhi was supported by the Dr. K.S. Krishnan Fellowship, Department of Atomic Energy, India. The authors are grateful to Prof. A.H. Chokshi for his suggestions and access to experimental facilities. The superalloy material was supplied by the Gas Turbine Research Establishment, Bangalore.

References

1. A.S. Gandhi, V. Jayaram and A.H. Chokshi, *Mater. Sci. Forum*, **243-245**, 227 (1997).
2. A.S. Gandhi, V. Jayaram and A.H. Chokshi, *J. Am. Ceram. Soc.*, **82**, 2613 (1999).
3. A.S. Gandhi, V. Jayaram and A.H. Chokshi, *Mater. Sci. Eng.,* **A304-306**, 785 (2001).
4. J. Frenkel, *J. Phys. (Moscow)*, **5,** 385 (1945).
5. J.K. Mackenzie and R. Shuttleworth, *Phys. Soc. (London)*, **62**, 833 (1949).
6. M.N. Rahaman, Ceramic Processing and Sintering, Marcel Dekker, New York, NY, USA, 374 (1995).
7. P. Murray, E.P. Rogers and E.A. Williams, *Trans. Br. Ceram. Soc.*, **53**, 474 (1954).
8. Y.-M. Chiang, D.P. Birnie III, W.D. Kingery, Physical Ceramics, John Wiley & Sons, New York, NY, USA, (1997).
9. G.W. Scherer, *J. Am. Ceram. Soc.*, **60**, 236 (1977).
10. Jagota and P.R. Dawson, *Acta Metall.*, **36**, 2551 (1988).
11. J.R. Matthews, *Acta Metall.*, **28**, 311 (1980).
12. Herring, *J. Appl. Phys.*, **21**, 301 (1950).
13. S.-J. Park, H.N. Han, K.H. Oh and D.N. Lee, *Intl. J. Mech. Sci.*, **41**, 121 (1999).
14. Paramanand and P. Ramakrishnan, *Powder Metall.*, 27, 163 (1984).
15. H.F. Fischmeister, E. Arzt and L.R. Olsson, *Powder Metall.*, **21**, 179 (1978).

16. R.W. Heckel, *Trans. Metall. Soc. AIME*, **221**, 1001 (1961).

17. R.L. Hewitt, W. Wallace and M.C. de Malherbe, *Powder Metall.*, **17**, 1 (1974).

18. A.S. Gandhi, Ph.D. Thesis, Indian Institute of Scienc, Bangalore, India (2001).

19. A.S. Gandhi and V. Jayaram, to be published.

20. R.M. German, Powder Metallurgy Science, Metal Powder Industries Federation, Princeton, NJ, USA, 221 (1994).

21. I. Shapiro and I.M. Kolthoff, *J. Phys. Colloid. Chem.*, **51**, 483 (1947).

22. K. Konopicky, *Radex Rundschau*, **3**, 141 (1948).

23. M.M. Carroll and K.T. Kim, *Powder Metall.*, **27**, 153 (1984).

24. H.F. Fischmeister and E. Arzt, *Powder Metall.*, **26**, 82 (1983).

25. A.R. Akisanya, A.C.F. Cocks and N.A. Fleck, *Int. J. Mech. Sci.*, **39**, 1315 (1997).

26. D.N. Lee and H.S. Kim, *Powder Metall.*, **35**, 275 (1992).

27. H.S. Kim, *Mater. Sci. Eng. A*, **A251**, 100 (1998).

28. X.-K. Sun, S.-J. Chen, J.-Z. Xu, L.-D. Zhen and K.-T. Kim, *Mater. Sci. Eng. A*, **A267**, 43 (1999).

29. H. Park and K.T. Kim, *Mater. Sci. Eng.*, **A299**, 116 (2001).

Figure Captions

Fig.1: SEM micrographs of the amorphous Z40A powders used in the hot pressing studies (a) coarse (C) with 17 μm average particle size, (b) Medium (M) with 3 μm average particle size and fine (F) with 1 μm average particle size.

Fig.2: SEM micrograph of powders used in the densification studies (a) the borosilicate glass powder with 9 μm average particle size and (b) silver powder with 2 μm average particle size.

Fig.3: Hot pressing of amorphous Z40A with the fine particle size. **The relative density was calculated based on 3.4 gcm^{-3} as the true density.** (a) The variation of relative density with continuously increasing uniaxial pressure. (b) Relative density at constant pressure of 750 MPa.

Fig.4: Densification curves for borosilicate glass powder, at 500°C. Relative density with increasing pressure (a), and with time at constant indicated pressure (b). It is clear that time dependent (viscous) densification is the dominant mechanism.

Fig.5: Cold compaction of silver powder up to 250 MPa shows large densification during pressurising. Relative density with increasing pressure (a), and with time at constant indicated pressure (b). Note the similarity with the hot compaction of amorphous ZrO_2-Al_2O_3.

Fig.6: The effect of particle size of amorphous Z40A powders on their densification behaviour, (a) 600°C, (b) 450°C and (c) 300°C.

Fig.7: Effect of cold compaction pressure on the densification behaviour during hot pressing of amorphous Z40A (F) at 600°C.

Fig.8: Comparison between the experimental and predicted uniaxial pressure for hot pressing of amorphous Z40A at 600°C. (a) Coarse powder and (b) fine powder.

Fig.9: Plots of the applied pressure against the quantity $\rho^2(\rho-\rho_0)/(1-\rho_0)$ where ρ is the fractional relative density. The hot pressing temperatures are (a) 600°C, (b) 450°C, and (c) 300°C. The presence of multiple consolidation mechanisms including significant plastic

deformation along with particle rearrangement and fragmentation are believed to lead to non-linear curves at the higher temperatures.

Fig.10: Hardness of hot pressed samples of amorphous Z40A as a function of hot pressing time at 600°C and a pressure of 750 MPa.

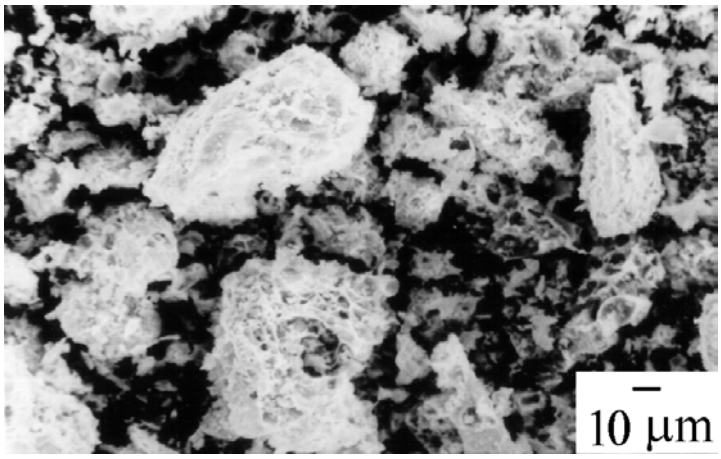

(a)

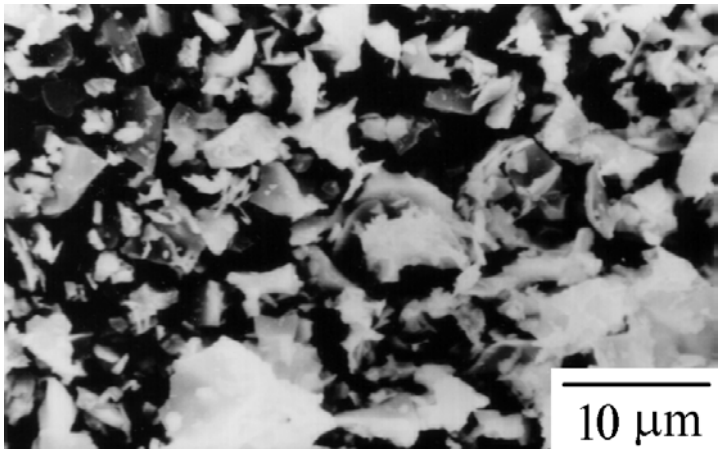

(b)

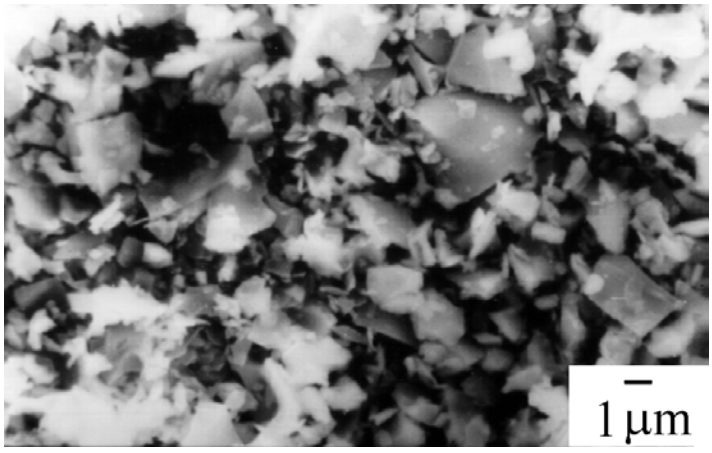

(c)

Fig.1

(a)

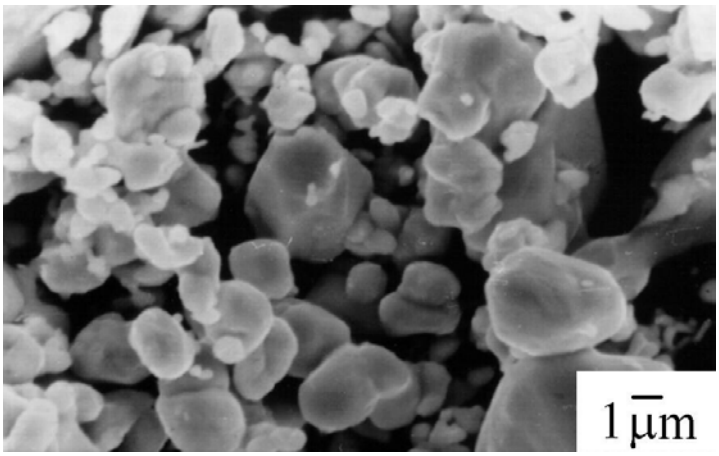

(b)

Fig.2

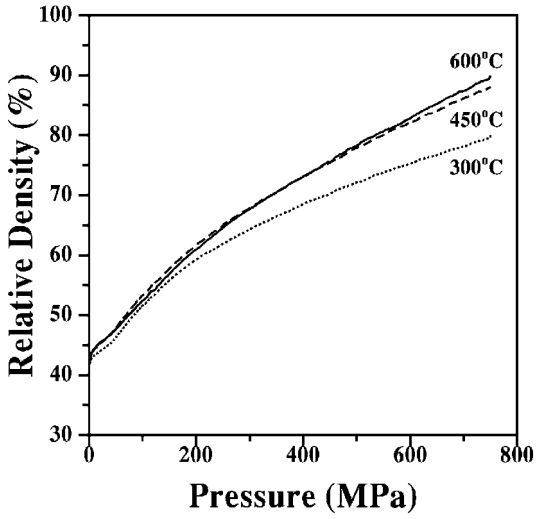
Relative Density (%)
Pressure (MPa)
600°C
450°C
300°C
100
90
80
70
60
50
40
30
0
200
400
600
800

(a)

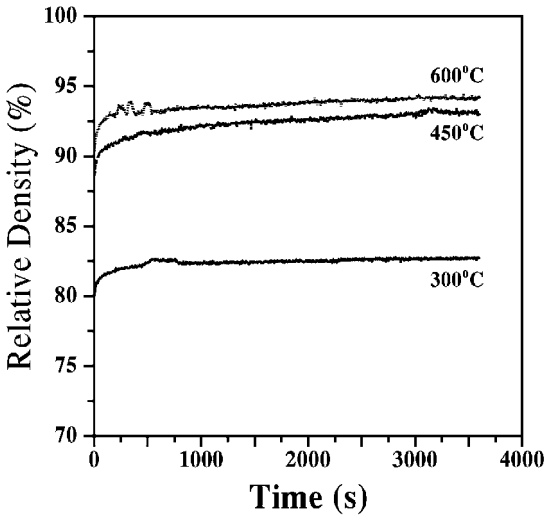
Relative Density (%)
Time (s)
600°C
450°C
300°C
100
95
90
85
80
75
70
0
1000
2000
3000
4000

(b)

Fig.3

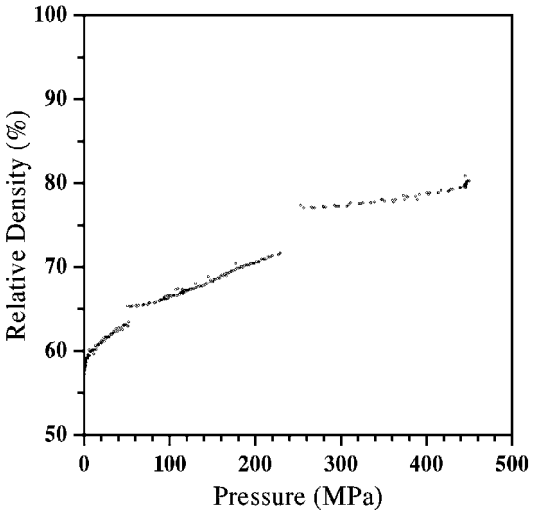
Relative Density (%)
100
90
80
70
60
50
0
100
200
300
400
500
Pressure (MPa)

(a)

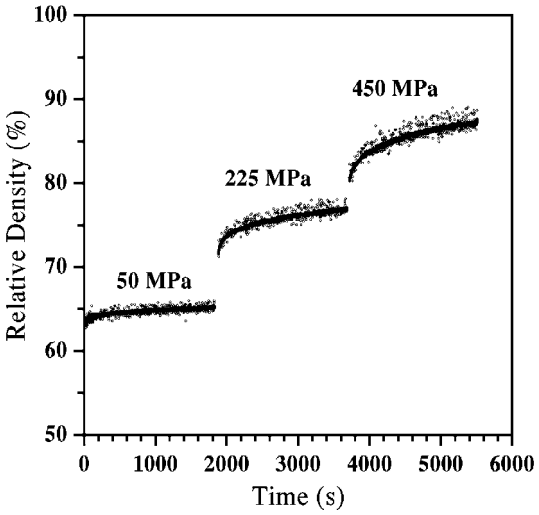
Relative Density (%)
100
90
80
70
60
50
450 MPa
225 MPa
50 MPa
0
1000
2000
3000
4000
5000
6000
Time (s)

(b)

Fig.4

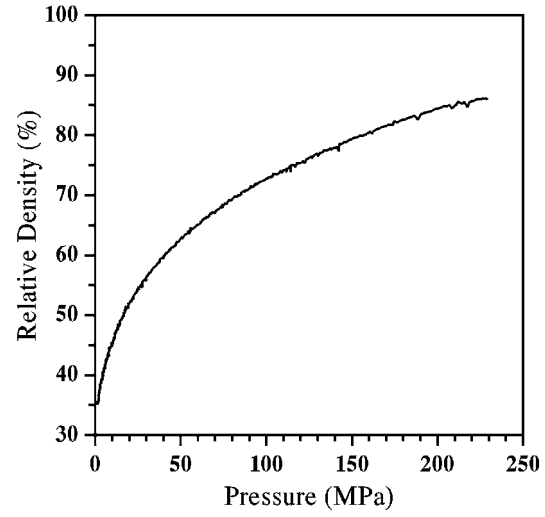
Relative Density (%)
Pressure (MPa)
100
90
80
70
60
50
40
30
0
50
100
150
200
250

(a)

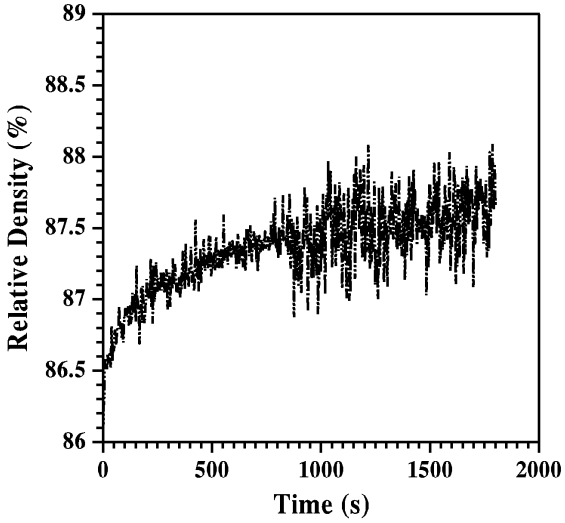
Relative Density (%)
Time (s)
89
88.5
88
87.5
87
86.5
86
0
500
1000
1500
2000

(b)

Fig.5

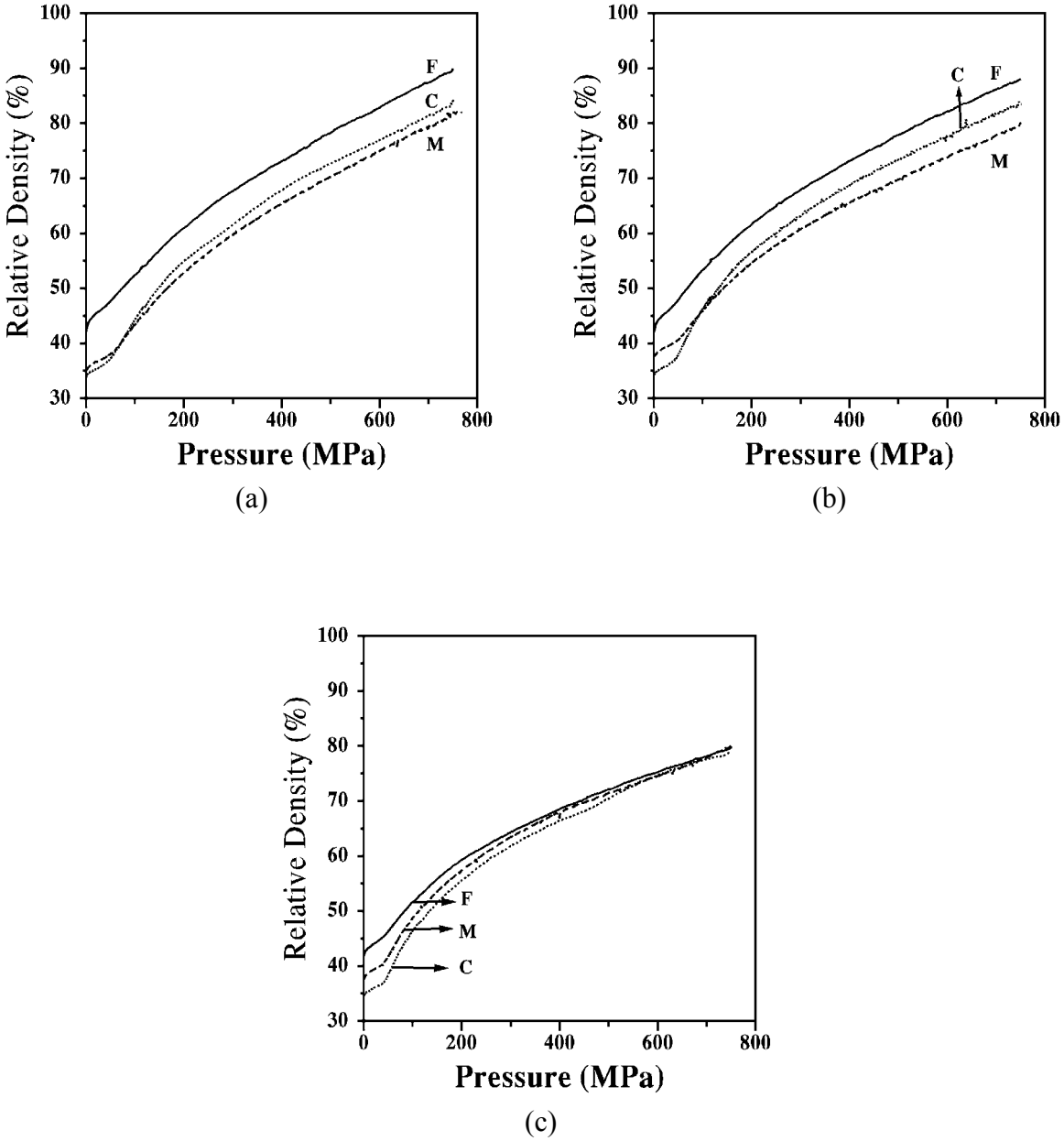

Fig.6

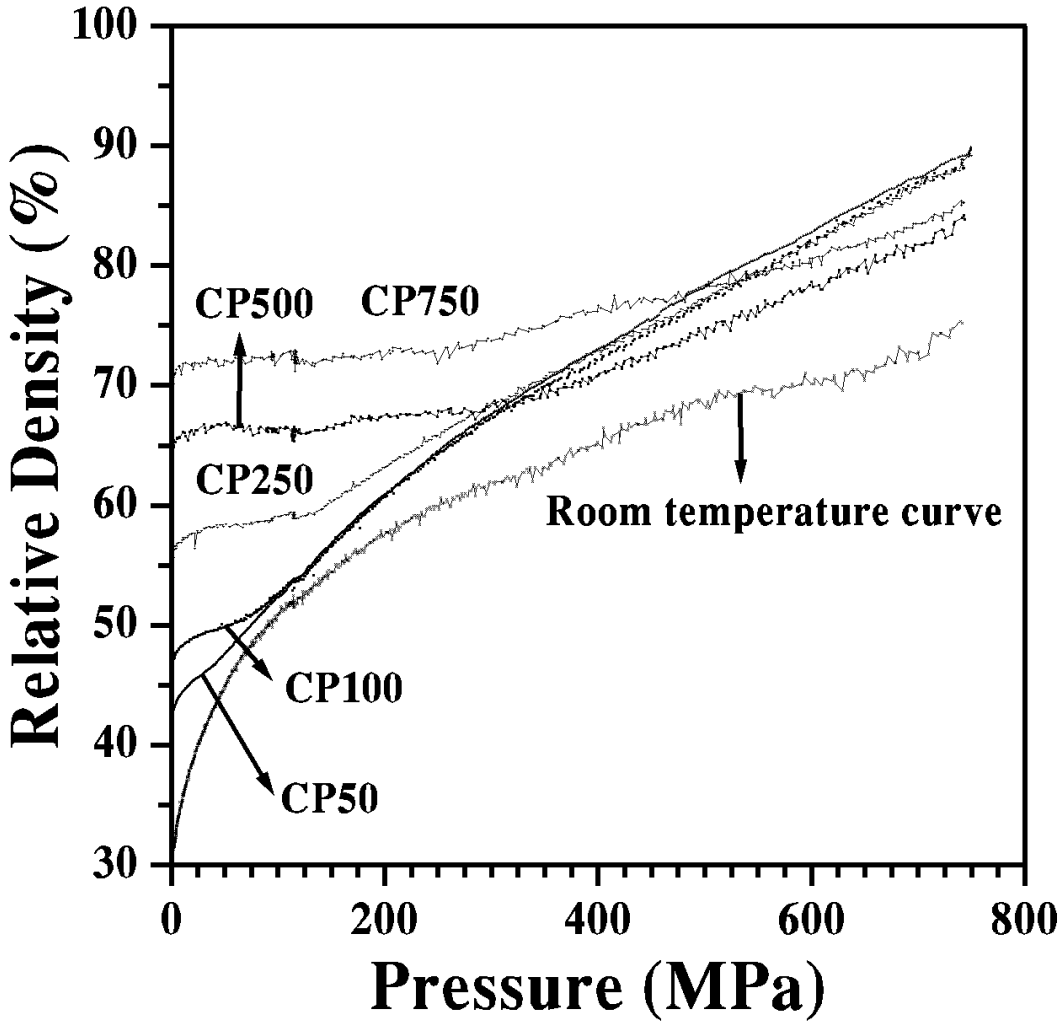
Relative Density (%)
100
90
80
70
60
50
40
30
0
200
400
600
800
Pressure (MPa)
CP500
CP750
CP250
Room temperature curve
CP100
CP50

Fig.7

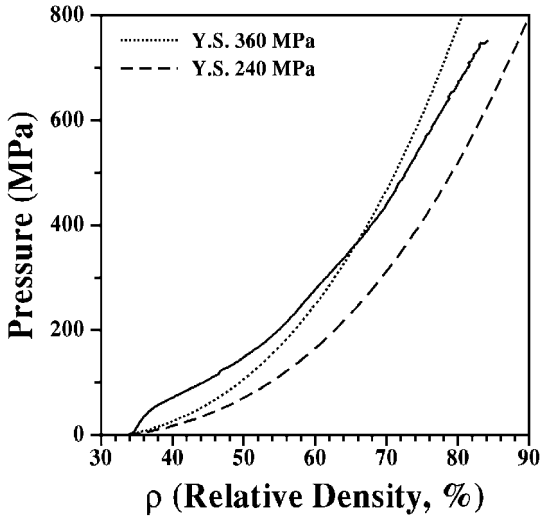
Y.S. 360 MPa
Y.S. 240 MPa
Pressure (MPa)
0
200
400
600
800
30
40
50
60
70
80
90
ρ (Relative Density, %)

(a)

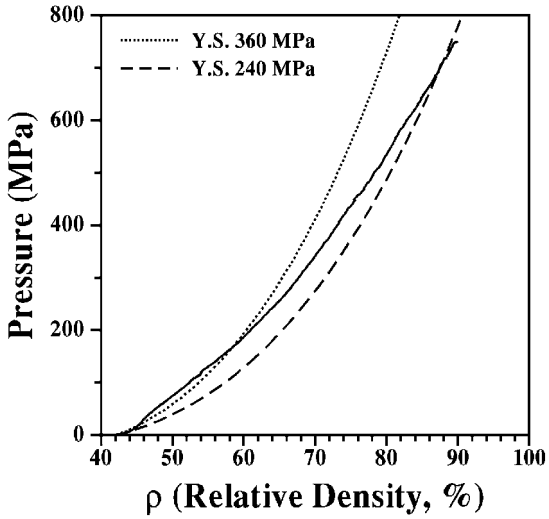
Y.S. 360 MPa
Y.S. 240 MPa
Pressure (MPa)
0
200
400
600
800
40
50
60
70
80
90
100
ρ (Relative Density, %)

(b)

Fig.8

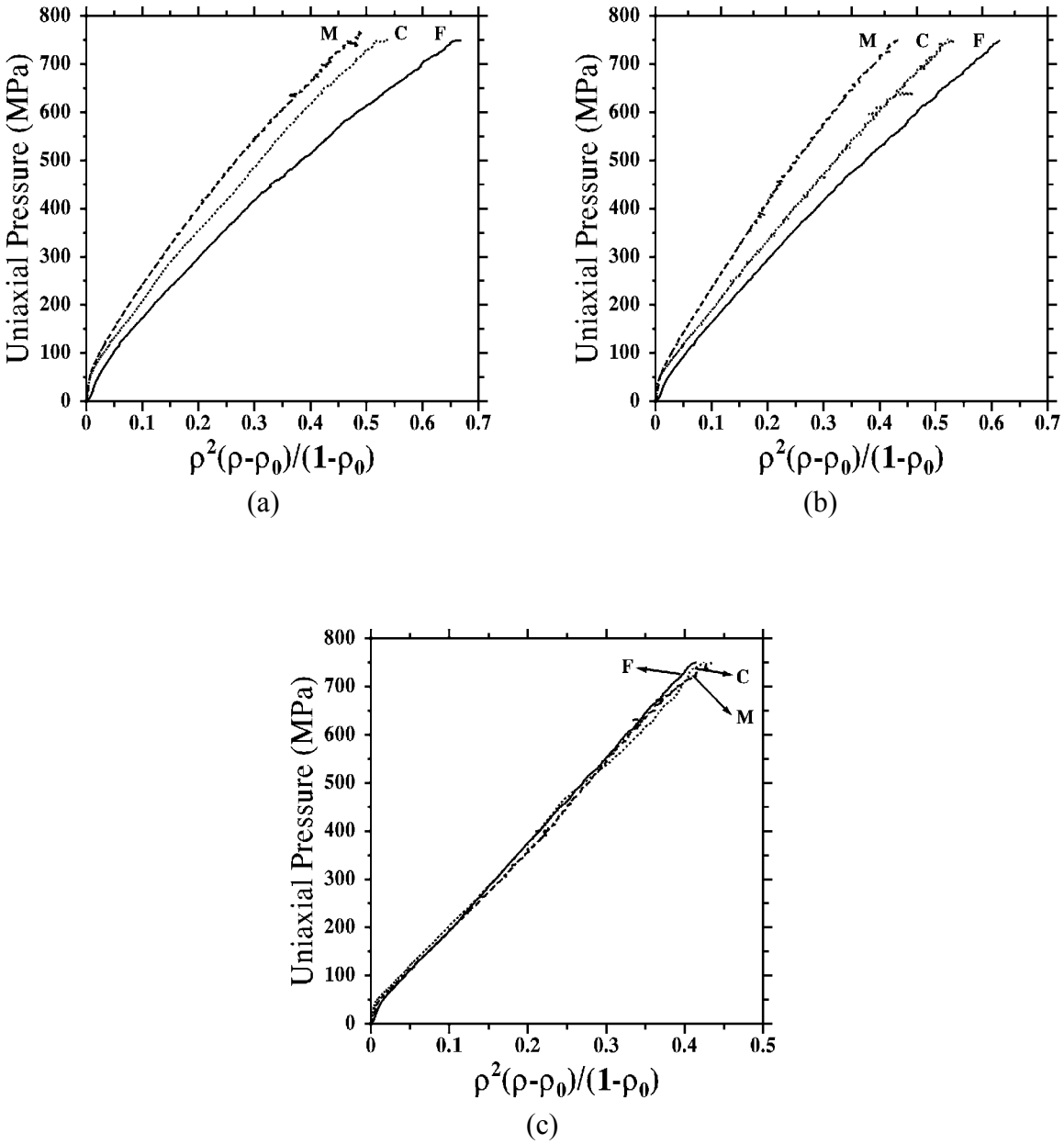

Fig.9

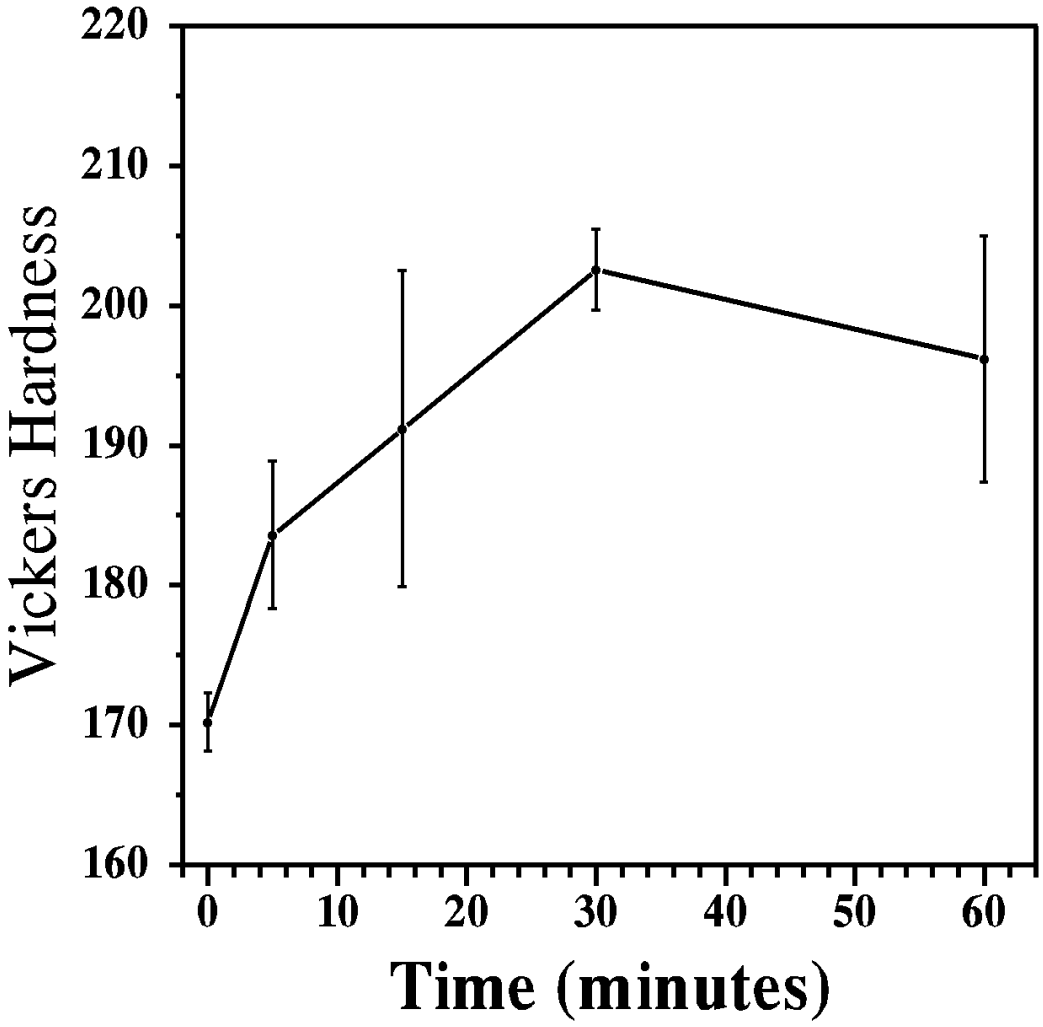
220
210
200
190
180
170
160
Vickers Hardness
0
10
20
30
40
50
60
Time (minutes)

Fig.10

1 A.S. Gandhi, V. Jayaram and A.H. Chokshi, *Mater. Sci. Forum*, **243-245**, 227 (1997).

2 A.S. Gandhi, V. Jayaram and A.H. Chokshi, *J. Am. Ceram. Soc.*, **82**, 2613 (1999).

3 A.S. Gandhi, V. Jayaram and A.H. Chokshi, *Mater. Sci. Eng.,* **A304-306**, 785 (2001).

4 J. Frenkel, *J. Phys. (Moscow)*, **5,** 385 (1945).

5 J.K. Mackenzie and R. Shuttleworth, *Phys. Soc. (London)*, **62**, 833 (1949).

6 M.N. Rahaman, Ceramic Processing and Sintering, Marcel Dekker, New York, NY, USA, 374 (1995).

7 P. Murray, E.P. Rogers and E.A. Williams, *Trans. Br. Ceram. Soc.*, **53**, 474 (1954).

8 Y.-M. Chiang, D.P. Birnie III, W.D. Kingery, Physical Ceramics, John Wiley & Sons, New York, NY, USA, (1997).

9 G.W. Scherer, *J. Am. Ceram. Soc.*, **60**, 236 (1977).

10 A. Jagota and P.R. Dawson, *Acta Metall.*, **36**, 2551 (1988).

11 J.R. Matthews, *Acta Metall.*, **28**, 311 (1980).

12 C. Herring, *J. Appl. Phys.*, **21**, 301 (1950).

13 S.-J. Park, H.N. Han, K.H. Oh and D.N. Lee, *Intl. J. Mech. Sci.*, **41**, 121 (1999).

14 Paramanand and P. Ramakrishnan, *Powder Metall.*, 27, 163 (1984).

15 H.F. Fischmeister, E. Arzt and L.R. Olsson, *Powder Metall.*, **21**, 179 (1978).

16 R.W. Heckel, *Trans. Metall. Soc. AIME*, **221**, 1001 (1961).

17 R.L. Hewitt, W. Wallace and M.C. de Malherbe, *Powder Metall.*, **17**, 1 (1974).

18 A.S. Gandhi, Ph.D. Thesis, Indian Institute of Scienc, Bangalore, India (2001).

19 A.S. Gandhi and V. Jayaram, to be published.

20 R.M. German, Powder Metallurgy Science, Metal Powder Industries Federation, Princeton, NJ, USA, 221 (1994).

21 I. Shapiro and I.M. Kolthoff, *J. Phys. Colloid. Chem.*, **51**, 483 (1947).

22 K. Konopicky, *Radex Rundschau*, **3**, 141 (1948).

23 M.M. Carroll and K.T. Kim, *Powder Metall.*, **27**, 153 (1984).

24 H.F. Fischmeister and E. Arzt, *Powder Metall.*, **26**, 82 (1983).

25 A.R. Akisanya, A.C.F. Cocks and N.A. Fleck, *Int. J. Mech. Sci.*, **39**, 1315 (1997).

26 D.N. Lee and H.S. Kim, *Powder Metall.*, **35**, 275 (1992).

27 H.S. Kim, *Mater. Sci. Eng. A*, **A251**, 100 (1998).

28 X.-K. Sun, S.-J. Chen, J.-Z. Xu, L.-D. Zhen and K.-T. Kim, *Mater. Sci. Eng. A*, **A267**, 43 (1999).

29 H. Park and K.T. Kim, *Mater. Sci. Eng.*, **A299**, 116 (2001).